Effects of Germanium, Copper and Silver Substitutions on Hardness and Microstructure in Lean Al-Mg-Si Alloys

Eva A. Mørtsell*[1], Calin D. Marioara[2], Sigmund J. Andersen[2], Jostein Røyset[3], Oddvin Reiso[3] and Randi Holmestad[1]

[1]Department of Physics, Norwegian University of Science and Technology (NTNU), 7491 Trondheim, Norway

[2]SINTEF Materials and Chemistry, N-7465 Trondheim, Norway

[3]Hydro Aluminum R&D Sunndal, N-6600 Sunndalsøra, Norway

*Corresponding author. E-mail address: eva.mortsell@ntnu.no

Abstract

It is shown that strength loss in a 6060 Al-Mg-Si alloy caused by reduction in solute can be compensated by adding back smaller quantities of Ag, Ge and Cu. Nine alloys were investigated. Ge was found to be the most effective addition, strongly refining the precipitation. The hardness is discussed in terms of statistics of the precipitates near a T6 condition, as acquired by transmission electron microscopy. Precipitates in some conditions were also investigated by high angle annular dark field scanning transmission electron microscopy. The added elements have strong influence on the main hardening precipitate, β', changing its structure and promoting disorder.

Keywords: Al-Mg-Si alloy, TEM, precipitation, Germanium, Silver, Copper

1 Introduction

The main use of 6xxx aluminum alloys is in extruded or rolled products. A very important issue is the ease with which they can be extruded. The aluminum companies have conducted much research to ensure that energy expenditure is low during extrusion and that the process is rapid without interruptions. Generally, solute additions decrease ductility and increase strain hardening rate and flow stress [1]. It is of advantage for optimal extrusion rates to limit the total amount of solute as well as the content of certain elements. Commercial alloys like AA6060, serving as the reference in this study, are already well optimized with regard to amount of solute and extrusion properties. An increase in extrusion speed achieved simply by reducing the amount of solute inevitably leads to a loss in strength. Here, we investigate a way to circumvent this: First, the overall amount of solute is reduced. Secondly, to compensate for the accompanied strength-loss, we add a small quantity with one or more of the elements Cu, Ge and Ag, which are known to have an effect on precipitation. How these additions effect the precipitate microstructure will be discussed with respect to hardness as well as to types, numbers and sizes of precipitates, as quantified by transmission electron microscopy (TEM).

The precipitation sequence in ternary Al-Mg-Si alloy may be given as [2]:

SSSS → atomic clusters → GP-zones (pre-*β''*) [3-4] → *β''* [5-6] → *β'* [7], *U1* [8], *U2* [9], *B'* [10] → *β*, Si (stable)

Where SSSS is the abbreviation for supersaturated solid solution. The precipitates are needles, laths or rods extending along <100>Al directions where they are fully coherent. The microstructure associated with maximum (or peak) hardness normally consists of a combination of very high numbers of finely dispersed GP-zones and *β''* type precipitates. For long ageing times other precipitates replace *β''*. These are of type *β'*, *U1*, *U2* and *B'*. These precipitates can grow to large sizes, and have a much lower hardening potential than *β''*.

The precipitation sequence changes with the introduction of strain [11-12] or the addition of other elements, such as Cu [13-16]. There are many studies with Cu, especially in the context of corrosion [17-19], but effects on the microstructure from Ag and Ge additions appear not to have been investigated for lean alloys like AA6060. The choice of Cu, Ag and Ge has been based on previous works, which show that they can improve material strength, at least in denser alloys [13, 20-21]. Other reasons concern similarities and differences of atomic size and electronic properties, and that all three elements are known to combine in - and modify - the precipitate structures. Recent studies show they interact with the solute clusters responsible for nucleation [22-24]. We are not aware of similar studies in high extrusion speed 6060 Al alloys where Ag, Cu, and Ge are added to compensate for property loss when total solute is reduced. Below we discuss the particular elements in some detail.

1.1 Copper

Cu is normally present in small amounts in Al-Mg-Si alloys, or added on purpose by industry because it is known to improve strength. However, amounts even as low as 0.1 wt % can cause problems with inter-granular corrosion [17-19]. The problem is related to the tendency of corrosion prone precipitate phases to form, especially the Q-$Al_4Mg_8Si_7Cu_2$ phase [25], which nucleates on grain boundaries [18]. It has also recently been found that Cu forms film-like enrichments along the grain boundaries, promoting inter-granular corrosion [19]. For these reasons, in the current study the maximum Cu level was set at 0.05 wt %.

Cu can substitute both Al and Si in the precipitate structures and in the interfaces [26-27]. For example, *Q'* and *Q* [25] are isostructural with *B'*, where Cu has substituted some partly occupied Al-positions [10]. Unlike the binary Al-Si system (or Al-Ge), where only pure Si (Ge) precipitates form, Cu combines with Al in the Al-Cu system, for example forming the hardening precipitates of type *θ'* - Al_2Cu [28]. For this reason alone Cu might be expected to have a strong effect on nucleation when added to other Al-based systems. In 6xxx alloys Cu suppresses the formation of pure *β''* by promoting disorder in the precipitate structures as well as inducing other precipitate types [13-16]. This is not necessarily a disadvantage as the new precipitates have hardening properties, and precipitate number densities and volume fractions do not decrease relative to total solute amount [13, 21].

1.2 Silver

A reason for adding Ag is that small additions in several age-hardenable Al based alloys containing Mg have been found to stimulate GP-zone formation and precipitation and generally to accelerate the kinetics of the age-hardening response and increase peak hardness [29-31]. For example, binary Al-Mg alloys with Mg below ~10 wt % are practically non-heat-treatable. By adding 0.5 wt % Ag a significant hardening response has been observed [31]. In pure form Ag, Al and Cu all form fcc structures. They have significant differences in bonding, which is quite obvious just by considering the composition of their normal oxides: Ag_2O, Al_2O_3 and CuO. Since Al and Ag are similar in size, precipitation may be compared in binary Al-Cu and Al-Ag alloys. Although the first precipitates to form in both systems are plates, in Al-Cu they form on {100} Al planes [32], while in Al-Ag they grow on {111} Al planes [33]. This shows that, even if Ag is more similar to Al than Cu regarding size and oxidation properties, Ag should not be considered a sole replacement for Al. In fact, electron microscopy has shown that in precipitates of the 6xxx system Ag occupies Al positions by enriching the matrix outside precipitates, as well as replacing Si-positions within the precipitate structures [34]. In Al-Cu-Ag, Cu and Ag are not found to mix well [35]. Here Ag only goes to precipitate interfaces or segregates in the matrix. According to Kim et al. the addition to dense Al-Mg-Si alloys of Ag, or Ag and Cu (with a total of about 0.10 at %) clearly affects the age-hardening behavior and increases peak hardness when the material is aged at 170 °C [20]. During over-aging, Ag causes β'_{Ag} to form, which has structure and composition differing from the normal β' phase in Al-Mg-Si alloys [34]. If similar size and same (fcc) structure as Al are the only criteria, more Ag in solid solution in a 6000 alloy is unlikely to require extra energy during extrusion. Recently, it has been found that elongation improves with Ag additions [36], a result which could indicate improved extrudability.

1.3 Germanium

Ge is chemically similar to Si, but is a larger and heavier atom. The replacement of Si with Ge in alloys richer in (Mg + Si) solute has been investigated in former studies [37-38]. One of the effects is a general refinement of the precipitation, with a following increase in hardness. When observed in the precipitate structures Ge has been found to occupy the same positions as Si. Just as Si it forms a hexagonal network of columns along <100>Al, which is well integrated in the matrix, and which is common for the Ge-Mg-(Al) containing precipitates. These two elements substitute each other in the network columns. Increasing the Ge amount seems to create more disordered precipitates on an otherwise ordered network. Full replacement of Si by Ge prevents the formation of the *β''* phase altogether. Instead, the material gains strength by precipitates isostructural to those of the ternary Al-Mg-Si system which are not normally associated with hardening; *U1*-like and *β'*-like precipitates are found alongside a high fraction of disordered precipitates [38].

When together with Cu, precipitates of the disordered *L*-phase of the Al-Mg-Si-Cu system [21] have been observed to dominate at peak hardness in an Al-Mg-Si-Ge-Cu alloy [39]. As a

direct cause of this phase, in a high-strength Al-Mg-Si-Cu alloy, when adding Ge in low concentrations (0.13 wt %), both thermal stability and peak hardness improved [21]. This work also showed that if only 10 % of the Si amount is replaced by Ge, precipitate number density increases quite significantly, and precipitates become finer. Ge is a useful substitution to investigate also because it gives a higher Z-contrast in high angle annular dark-field scanning TEM (HAADF-STEM) experiments.

1.4 Vacancies and dislocations

For an alloy pair, where one alloy contains less solute than the other, but where heat-treatments are identical, more quenched-in vacancies per solute atom should be expected in the leanest alloy. Excess of quenched-in vacancies is known to form various clusters and voids, of which 'prismatic clusters' of vacancies were experimentally shown as early as 1958 [40]. They were later found to be loops of dislocations called 'Frank loops' [41]. Recent calculations support the observations, for example showing that only a few vacancies clustering on a (111) Al plane can form a prismatic dislocation loop [42]. A good introduction with further references can be found elsewhere [43]. Clusters of vacancies and dislocations clearly will influence nucleation. Dislocations normally lead to more inhomogeneous precipitation. Dislocation loops as well as the vacancies attract solute atoms and may be the sources for clustering. However, dislocations aid also in annihilating vacancies, while (some) solute atoms and vacancies may form bonds which should reduce the concentration available for forming the voids and dislocations in the first place. As has been suggested previously, e.g. by Kubota et al. [31], adding elements which bond vacancies should be expected to reduce the ability to form loops, thereby reducing dislocation density.

A recent work [44] shows that vacancy binding energy for the current alloying elements increases with the elements Mg, Cu, Si, Ag, and Ge. Mg has very weak binding energies. In some calculations it was found to be even weakly negative. Binding energy generally increases with size. However, since atomic radius increases as Si, Ge, Cu, Al, Ag, and Mg size cannot be the only factor [44]. The higher solute-vacancy binding energy means vacancies surround Ge and Ag more than the other atoms. Ge is chemically similar to Si, but also larger. As mentioned, Si and Ge substitute each other in the columns of the precipitates which define the Si-network. Ag and Cu also can enter these columns to some extent. Since the network is an integral part of all precipitates it is reasonable to think these elements are already in the clusters in the early stages of precipitation. The prevalence of the network means it must be initiated early, which means Si has an important role from the very start. Since Ge, Ag and Cu could all be substituting Si atoms in the clusters, the difference in attraction to vacancies is likely to change the kinetics of the clustering. For example, this may be the reason a small substitution of Si by Ge in denser alloys refines the precipitate microstructure [21]. It has been speculated that the reason Mg and Si combine in clusters, is to cancel the differences in the vacancy binding energy [44]. This tendency should therefore be stronger when Ge replaces Si, which can explain its refining effect [21]. A further support is the observation that Ag and Mg form initial clusters in an Al-Cu-Mg-Ag alloy [45].

2 Method

A set of nine high purity alloys were produced with the compositions shown in Table 1, as measured by inductively coupled plasma optical emission spectroscopy. The Al base metal had a purity of 99.9 wt %. The effective solute (S_{eff}) available for precipitation is defined by the sum Mg + Si* + Cu + Ge + Ag. The asterisk indicates that an amount of Si must be subtracted from the tabulated value as it is consumed by iron-rich phases. In Al 6060 the difference is estimated to equal one quarter of the wt % of Fe [46]. The effective Si content (Si*) for an alloy is therefore 0.05 wt % (0.048 at %) less than what is given in Table 1. The last column of the table gives the overall reduction in effective solute, as per cent of atomic and mass content compared to alloy RX0, which is the dense reference with composition near a commercial 6060 Al alloy. RX1 is a leaner reference, but the solute mass (Mg + Si) is reduced by 16.8 wt % (16.7 at %).

Table 1 Alloy composition, effective solute (S_{eff}) and solute reduction ΔS relative to RX0

Alloy	Si[a]	Ge	Mg	Cu	Ag	Fe	Mn	S_{eff} [b]	ΔS[c] (- %)
RX0wt%	0.45	–	0.37	–	–	0.20	0.03	0.77	–
RX0 at%	0.43	–	0.41	–	–	0.10	0.015	0.80	–
RX1 wt%	0.37	–	0.32	–	–	0.20	0.03	0.64	16.8
RX1at%	0.36	–	0.36	–	–	0.10	0.015	0.66	16.7
RXGC1 wt%	0.37	0.05	0.32	0.05	–	0.20	0.03	0.74	3.9
RXGC1 at%	0.36	0.02	0.36	0.021	–	0.10	0.015	0.70	11.6
RXAC1 wt%	0.37	–	0.32	0.05	0.08	0.20	0.03	0.77	0
RXAC1 at%	0.36	–	0.36	0.021	0.02	0.10	0.015	0.71	11.4
RXG2 wt%	0.35	0.10	0.30	–	–	0.20	0.03	0.70	9.1
RXG2 at%	0.34	0.04	0.33	–	–	0.10	0.015	0.66	17.1
RXGC2 wt%	0.35	0.05	0.30	0.05	–	0.20	0.03	0.70	9.1
RXGC2 at%	0.34	0.02	0.33	0.021	–	0.10	0.015	0.66	16.9
RXA2 wt%	0.35	–	0.30	–	0.10	0.20	0.03	0.70	9.1
RXA2 at%	0.34	–	0.33	–	0.025	0.10	0.015	0.65	18.7
RXAC2 wt%	0.35	–	0.30	0.05	0.05	0.20	0.03	0.70	9.1
RXAC2 at%	0.34	–	0.33	0.021	0.013	0.10	0.015	0.66	17.6
RXGAC2 wt%	0.35	0.03	0.30	0.03	0.03	0.20	0.03	0.69	10.4
RXGAC2 at%	0.34	0.011	0.33	0.013	0.008	0.10	0.015	0.65	17.9

[a] Effective Si available for precipitation (Si*) is tabulated with an amount 0.05 wt % less[46]. [b] Effective solute S_{eff} = Mg+Si*+Ge+Cu+Ag. [c] Removed solute fraction as percentage of content in RX0. RX0 is the AA6060 reference alloy. RX1 is the leaner reference. 'A', 'C', or 'G' signify Ag, Cu, or Ge respectively. In alloys with Ag, Cu, or Ge numbers '1' or '2' signify high (0.74-0.77 at %) or low (0.67 - 0.69 at %) amount of total solute, respectively.

The remaining alloys have equal or less solute than RX0, and may be considered as heavier variants of RX1 with additions that are combinations of Ge, Cu, and Ag. The amount of any

of these elements is below 0.1 wt %. The sum of (trace) elements other than those listed in Table 1 was found to be below 0.01 wt %. Compared to RX0 the solute mass is reduced from 0 to10.4 % in the alloys with additions. In atomic percent the reductions are larger (11.4 to 18.7), depending on the elements. In spite of the large solute mass reduction, RX1 still has a comparatively high effective atomic solute content: Only the alloys RXGC1 and RXAC1 contain more. The alloy set allows for comparison regarding changes to solute mass as well as to atomic content. For example, there is no mass loss of solute from RX0 to RXAC1even if the solute atomic content has been reduced by 11.4 %. The alloys were cast in cylindrical billets of 4 kg, homogenized at 575 °C for three hours and then air cooled to room temperature (RT) within 1 – 2 hours before extrusion. Preheating to extrusion was done at 540 °C to ensure complete solid solution, and the extrudates were water-quenched within 5 seconds after extrusion. The alloys were extruded as round profiles of 2 cm diameters. 1 cm long samples were cut perpendicular to the extrusion direction. The heat treatment is shown in Fig. 1. The samples were solution heat treated (SHT) for 5 minutes in an air circulating furnace after reaching a temperature of 535 °C. Next, the samples were water quenched to RT and held at this temperature, i.e. naturally aged (NA) for 4 hours, where after they were artificially aged (AA) at 195 °C. They were heated to the AA temperature from room temperature in a non-linear manner that mimics industrial practices, with an average heating rate of 26 °C/hour. After suitable heat-treatment times (0, 1 h, 2 h, 4 h, 8 h, 16 h and 32 h AA at 195 °C) the samples were removed from the oven and immediately water quenched to RT, where the first time ('0') denotes the start of the heat treatment when 195 °C is first reached.

To improve contrast of the indentations, prior to every set of Vickers hardness (HV) measurements, samples were polished with SiC paper up to a fineness of 2500 #/cm^2. The hardness for each condition is given as an average of 10 indentations, the set consisting of five indentations from each side of the sample. The hardness curves are presented in Fig. 2.

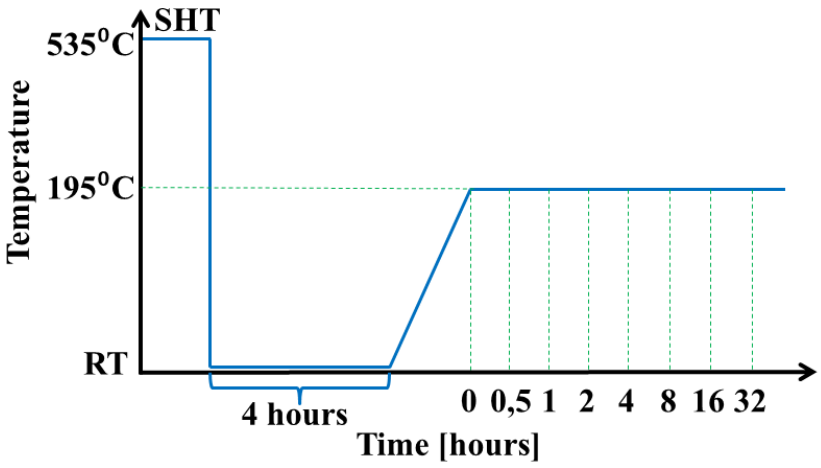

Fig. 1 Heat treatment overview. After quenching from solution temperature (535 °C), samples were held 4 hours at RT before taken to the 195 °C ageing temperature (26 °C/hour). Vertical dotted lines (with respective ageing times), indicate water-quenching to RT.

As observed in Fig. 2, for the three strongest alloys peak hardness arrives after 4 hours of AA. This condition was chosen for the TEM investigations of all the alloys. Thin foils for TEM specimens were prepared by polishing slices with surface normal parallel to the extrusion direction, down to about 100 μm. Disks of diameter 3 mm were stamped out from the foils. TEM specimens were prepared by using a twin-jet Tenu-Pol 5 electropolisher from Struers. The electrolyte consisted of 33 % nitric acid and 67 % methanol and was kept at temperatures ranging from - 30 °C to - 25 °C, controlled by adding liquid nitrogen to the solution. Bright field TEM images were acquired in a Philips CM30 TEM operated at a voltage of 150 kV. Parallel electron energy loss spectroscopy (PEELS) was used to obtain the thickness corresponding to each imaged area. A more detailed description of the method describing how to calculate precipitate needle cross sections, lengths, number densities and volume fractions can be found elsewhere [47].

Table 2 gives quantified parameters for the precipitates in the different alloys. Number densities and measurements of mean length are based on images similar to the ones shown in Fig. 3, while examples of images for needle cross-section measurements are shown in Fig. 4. Images for number densities are from regions away from grain boundaries and larger particles, meaning precipitates are always counted in the interior of a grain. The mean number density is based on counts of precipitates in 10 images (data sets) but from one grain only. The thickness (in the center of an image) varied from 70 to 150 nm. Experience has shown that number densities in homogeneous regions in the interior of grains vary little from grain to grain in the same alloy. Several grains were inspected to make sure the images came from representative areas. At least 1000 needles were counted for each alloy for the calculation of number density, 500 needles for obtaining average needle length, and a minimum of 50 cross section areas for estimating average cross section. As an exception, the precipitate density of RX1 is based on 20 images in two grains, because this alloy was the only one with an inhomogeneous precipitate distribution. In spite of this, the mean needle length and cross section were found to be similar in the different areas. The HAADF-STEM images were recorded with a spherical aberration (Cs), probe-corrected JEOL ARM200F. The probe size was 0.08 nm and the inner collection angle was 50 mrad.

3 Results and Discussion

The evolution of hardness in the nine alloys during the aging at 195 °C up to 32 hours is shown graphically in Fig. 2. Quantified parameters of the hardening precipitates are given in Table 2 for the 4 h AA condition that was investigated by TEM. This ageing time coincides with peak hardness for the three strongest alloys (RX0, RXG2 and RXGC1). The hardness maximum for most other alloys arrives at least one hour later. It was decided to characterize all the samples for identical heat-treatments rather than for times corresponding to individual hardness peaks, since the different solute elements and amounts will give hardness curves of different shapes.

3.1 General comparison

Fig. 2 shows that the hardness at the start of ageing (0 h AA) varies considerably among the alloys, ranging from 35 to 70 HV. The alloys generally keep their rank in hardness throughout the ageing, with the curves approaching each other at longer times. The strongest alloys reach peak hardness sooner than the weaker ones and show signs of faster over-ageing.

As the ageing proceeds, the curves tend to settle into two main groups; a high hardness group of alloys containing Ge but not Ag with the dense reference RX0 on top, and a low hardness group consisting of RX1 together with alloys containing Ag but not Ge. It is quickly verified that Cu improves the alloys with Ag, and may possibly also have an effect on the Ge alloys. However, the Cu-free alloys RXA2 and RXG2 range in both ends of the scale.

There are clear differences in the ageing curves of the two reference alloys: In Fig. 2 the densest alloy is the 6060 reference RX0. Its hardness is rivalled only by RXG2, while the leaner reference RX1 defines the bottom together with RXA2. Prior to discussing these two pairs in detail we compare the reference alloys.

3.2 The reference alloys

The effective solute in RX0 is 0.80 at %, compared to 0.66 % for RX1. After 4 h AA the respective precipitate volume fractions are measured to about 0.7 and 0.15. Comparing the curves of RX0 and RX1 in Fig. 2, we see that the hardness for RX1 at the start of the ageing is about half that of RX0. Strikingly, the number density of RX0 is about twenty times that of RX1, yielding a volume fraction at least four times higher. It is obvious that a much higher number of clusters must have developed into precipitates in RX0 during the ageing than in RX1. Fig. 2 also shows that RX0 reaches maximum faster than RX1.

The two curves continue almost in parallel up to about 60 minutes of AA. The bright field TEM images of the precipitates in Fig. 3 (a-b) and Fig. 4 (a-b) show that the same precipitate type is responsible for hardness in both alloys, namely *β”*. In RX0 [Fig. 3(a)], practically all needles lying in the viewing plane can be identified by pairs of dark lines. These 'double contrasts' are hall-marks of precipitates like *β”* (and pre-*β”* GP-zones). They originate from electrons scattered away from the direct beam on each side of a needle because of the surrounding cylindrical strain field. In RX1 [Fig. 3(b)] only some of the precipitates have the double contrasts. Absence of the strain field points to structures such as *β’*, *U2*, or *B’*. Fig. 4 (a-b) shows examples of precipitate cross-sections in the two alloys using higher magnification. Here we find rhomb-shaped precipitate cross-sections with uniform contrast, confirming that alloy RX0 must be dominated by *β”* needles. In (b) there are coarser, irregular precipitate cross-sections often containing a rhombic part similar to (a). These needles may be defined as disordered, with domains of several precipitate structures, but where one domain is ordered *β”*.

In RX1 the maximum hardness arrives later. This is likely to be caused by a combination of less solute (slower precipitation kinetics) and influence from other precipitate types, which

tend to form after β'' during ageing (post-β'' phases) and have different maxima and less strengthening potentials.

Unlike the other alloys, RX1 was found to have a considerable amount of dislocations and an inhomogeneous precipitate distribution with coarse precipitates decorating dislocation lines and finer precipitates in areas between. The densities were not quantified. However, this is similar to what was found by Kubota & al. [31] when comparing two Al-5 wt % Mg alloys, where one had 0.4 wt % Ag: the alloy with most solute (and Ag) had less dislocations. A higher dislocation density will explain the dual precipitate size distribution in alloy RX1. Examples from the two areas of RX1 are given in Fig. 5 (a-b), where (a) is in an area with less dislocations. The precipitates forming on the dislocations were not studied explicitly. However, it is well known that dislocations promote β' as well as the B' phase [11, 48]. In these situations the precipitates can have quite large cross-sections, and much disorder.

Since all the alloys were quenched from the same solution temperature they should have the same amount of excess vacancies. Although RX0 has the lowest solute weight, measured in atomic percent, five of the alloys have the same or less solute. These alloys did not show signs of inhomogeneous precipitation. We propose the coarser microstructure and apparent higher dislocation density in RX1 are results of the higher effective concentration of vacancies due to the lower overall amount of solute and the absence of Ag and Ge, elements which bind more strongly with vacancies than Mg and Si.

3.3 Effect of silver, the two alloys RX1 and RXA2 with lowest hardness

Figs. 3 (b) and (i) show respective images of the microstructure of RX1 and RXA2 [see also Figs. 4(b) and (c)]. Their hardness curves can be said to overlap throughout the ageing. On low magnifications their precipitate microstructures appear somewhat similar, although Table 2 shows that RX1 has the coarsest precipitates of all the alloys. No other alloy has a lower number density or longer needles, while average size of the cross-sections is the second largest. This results in a very low volume fraction of precipitates. The last column of Table 1 shows that, owing to the high atomic number of silver, the solute reduction in mass is much larger for RX1 than for RXA2 while the reduction in atomic content is largest for RXA2. In fact, RXA2 has the lowest amount of solute of all the alloys, and might therefore have been expected to obtain the lowest hardness of the two, especially since the content of Mg + Si is also less. Still, the number density in RXA2 is twice that of RX1 and the precipitates are slightly shorter. Since the mean precipitate cross-section in RXA2 is the largest of all alloys, it results in similar volume fractions for the two alloys. This indicates a benefit of adding Ag, especially since RXA2 is so low in solute. The higher number density in alloy RXA2 could therefore be a result of Ag contributing in formation and stabilization of clusters (co-clustering with Mg [45]) because of a higher binding energy to vacancies than Mg and Si. As previously suggested [31], Ag-vacancy complexes are likely to be attractive for other solute elements, thereby aiding nucleation. As can be seen in the HAADF-STEM images in Fig. 6 (a-b), silver enters the particles, but substitutes also in the Al fcc matrix just outside the particles. This image confirms that the major parts of the particles contain domains of β'', co-existing with domains of β'_{Ag} in the same needle [34]. Like the β'-phase in ternary Al-Mg-Si

β'_{Ag} has roundish cross-sections. This signifies limited lateral coherency and quicker coarsening, which probably explains the large average cross-sections observed in RXA2.

3.4 Effect of Germanium, the two alloys RX0 and RXG2 with highest hardness.

From Table 1 it can be seen that the solute content in RXG2 has been reduced with 17 at % relative to RX0, when including the 0.04 at % Ge added back. Still, this pair's hardness curves in Fig. 2 show a near overlap throughout the ageing. According to Table 2, RX0 has about twice the volume fraction of precipitates compared to RXG2 after 4 hours of ageing. The similar hardness arises since RXG2 has about 4 times the number density and precipitates have much smaller lengths and cross-sections. Figs. 3(a) and (d) illustrate the microstructures of RX0 and RXG2, respectively. The precipitate fineness in RXG2 is remarkable. The needles in the viewing plane appear as double line contrasts. However, the small cross-sections mean the lines of the pairs are often hard to separate visually. The HAADF-STEM image in Fig. 6(c) shows the cross-section of a needle in the RXG2 alloy. It is evident that this particle has strong similarities to *β''*, evidenced by the molecular *β''*-unit (indicated by a circle). In *β''* these units are stacked periodically along Al <310> and <320> directions. In the current case the particle contains stacking faults. The occasional brighter contrasts on the right hand side of the particle are evidence for (partial or full) Ge occupation in Si columns. The left side of the particle is more Ge rich. Here we see signs of a hexagonal ordering of Ge columns. This means that most of this particle is Ge-containing *β''*, more or less correctly stacked, seamlessly integrated with fragments of other more Ge-rich precipitate structures. The structural details are complex and besides the aim of this paper.

Less solute normally correlates with a lower number of coarser needles. The current case is different. The introduction of Ge clearly is causing the much higher precipitate number density after 4 hours of ageing. About four times more clusters nucleate the hardening phase in RXG2 than in RX0. It is unclear whether Ge initiates more clusters, stabilizes a higher proportion, or performs both tasks. Since Ag had a much weaker effect we propose the reason is chemical similarity with Si combined with larger size. Chemical similarity means Ge tends to form or participate in the same atomic arrangements as Si, also on the cluster level. Mg atoms have a low vacancy binding energy compared to Ge. Due to the much higher density of precipitates caused by Ge addition or substitution, this strongly suggests that Mg has a stronger adherence to Ge-containing clusters than to those only containing Si. We therefore suggest the reason for the high nucleation efficiency of Ge is the chemical resemblance to Si, enabling it to form the same stable structures based on the hexagonal Si/Ge network, as well as a higher vacancy binding energy.

The effective volumes of Mg and Si in the Al matrix were recently calculated by Leyson et al [49]. While Si is smaller than Al, Mg is larger. Both situations are energetically unwanted. However, if Mg and Si pair up they partly would cancel the volume dissimilarity with the Al matrix. This translates into saying the probability of these two elements staying together increases. In turn this should lower the probability of either element interacting with vacancies, which means diffusivity also becomes reduced. With the same logic, since Ge has a larger volume compared to Si, Ge and Mg would have a lower probability of pairing up as

compared to Si and Mg. In addition, Ge pulls strongly on vacancies [44]. Exchanging some Si with Ge could therefore have a double benefit: The activity increases because of a higher affinity for vacancies, and less of the cluster-forming diamond elements are bound up in pairs. The presumed Mg-Si pairing could be seen as a slowing down of the kinetics, as they are less able to attract other atoms and develop into clusters. The higher affinity the less bound Ge atom has for vacancies together with a chemical similarity with Si, seem to be the reasons behind its refining influence of the microstructure. This would also explain why Ge is localized mostly in the center of the precipitates and not towards the surfaces.

3.5 Effect of Cu in the Ag-containing alloys RXAC1 and RXAC2

The Cu-free alloy RXA2 [Fig. 3(i)] was discussed above in relation to the leanest reference RX1 [Fig. 3(b)]. These two alloys had the lowest amount of solute of all alloys. Alloys RXAC1 and RXAC2 are modifications of RXA2 with 0.05 wt % Cu. Micrographs are shown in Fig. 3 (g) and (h), respectively. From these images it is not evident that needle coarseness increases towards right (as g-h-i). This is consistent with the fact that RXAC2 is very low in solute, barely higher than RXA2. On the other side, only the rich reference (RX0) has more solute than RXAC1. Since RXAC2 is so low in solute it is no surprise its hardness curve (Fig. 2) is consistently below that of RXAC1. However, given the total amount of solute it is interesting that the curves are so close. Because of the identical level of Cu in the two alloys, the reason for the small difference cannot be explained by the absolute content of this element. Still, since both curves are above RXA2, this shows Cu has some beneficial effect. RXAC2 is most similar to RXA2, but precipitates in RXAC2 have a noticeable smaller cross-section. These two alloys have the same amount of Mg and Si as well as similar total solute. From RXA2 to RXAC2 the replacement of some Ag with Cu clearly has resulted in a reduction in precipitate cross-section.

The improvements in RXAC1 are more obvious. Relative to RXAC2, the number density increases by a factor of 5, while precipitates are strongly refined. This result may be understood by the higher amount of effective solute in RXAC1 (0.71 at %) as compared to RXAC2 (0.66 at %), referring to increases both in Mg + Si and in Ag. As discussed above, both these increases indicate more solute-vacancy bonding, and correlate with finer and more precipitates.

The identical levels of Mg and Si in reference RX1 and in RXAC1 mean these alloys are directly comparable. From Table 2 it can be observed that RXAC1 has a tenfold increase in number density together with a 50 % reduction in needle length and a 25 % reduction in cross-section area as compared to RX1. This is clearly the effect of the combined additions of Ag and Cu in RXAC1.

3.6 Effect of Cu in the Ge-containing alloys RXGC1 and RXGC2

From Fig. 2 it is seen that alloys RXGC1 and RXGC2, with reductions in atomic content of 11.6 and 16.9 % relative to the reference RX0, have hardness curves below RXG2 (with 17.1 % solute reduction). Since the Cu content is the same for both Cu-added alloys, and they have equal or more Mg + Si as compared with RXG2, the drop in hardness must be a direct

consequence of the reduction in Ge (0.04 at % in RXG2 to 0.02 at % in RXGC1 and RXGC2). That RXGC2 has lowest hardness of the two Cu-added alloys must be related to its lower content of Mg + Si. The main difference between the strongest alloy (RXG2) and the weakest alloy (RX1) is the 0.4 at % Ge content in RXG2. The most pronounced result of the Ge addition is a near 80-fold increase in number density, from 170 to 13200 per μm^3. When half of the Ge is substituted by Cu, RXGC2 still has the second highest number density of all the alloys (11200 μm^{-3}). The cross-sections and lengths decrease as the series RXGC1, RXGC2, and RXG2, while number densities increase.

It is evident that Cu does not refine cross-sections much, at least compared to Ge: substituting half the Ge by Cu (from RXG2 to RXGC2) resulted in lower density of coarser needles and a significant loss of hardness. The higher precipitate number density in RXGC2 as compared to RXGC1 is probably a consequence of the increased Ge level, while the higher precipitate volume fraction in RXGC1 might be caused by its higher amount of Mg + Si.

After 4 hours ageing the hardness of these three alloys is similar. It is possible a different ageing treatment could change the ranking.

3.7 Cu, Ge and Ag together: Alloy RXGAC2

Alloy RXGAC2 has similar Mg + Si and overall solute amount as all the alloys having designations ending with '2', and contains additions of all Ag, Cu, and Ge. However, for each of the three elements the addition is lower than in any of the other alloys. In spite of this, RXGAC2 has higher hardness than alloys RXA2 and RXAC2. This underlines the beneficial effects of adding small amounts of Ge (0.011 at %), explaining why RXGAC2 compares in hardness with RXAC1 in spite of its lower Mg + Si and total solute content. Table 2 shows that the microstructure in RXAC2 after 4 h AA is finer compared to that in RXA2 and RXAC2, although it is similar to the microstructure of RXAC1. An HAADF-STEM image of a precipitate from RXGAC2 in Fig. 6(b) shows that it contains a *β''* part and a disordered part fused in the same needle, with the high Z-contrast added elements localized in the disordered part. This is similar to the observations in Fig. 6(a, c) from alloys RXA2 and RXG2.

Regarding the Cu and Ag additions, it should be noted that their concentration in the present alloys are half or less as compared to the alloys in references [20] and [50], which might explain the generally weak influence on hardness and microstructure. Such additions seem to work better in denser alloys. This can be observed by comparing the microstructure data of alloys RXAC1 and RXAC2 in Table 2, showing that the denser alloy RXAC1 has a higher precipitate number density than RXAC2. By contrast, alloy RXGC2 has a similar solute level as RXAC2, practically the same amount of Cu, but with Ge instead of Ag. Here we can clearly see a high increase in precipitate number density correlating with increased hardness.

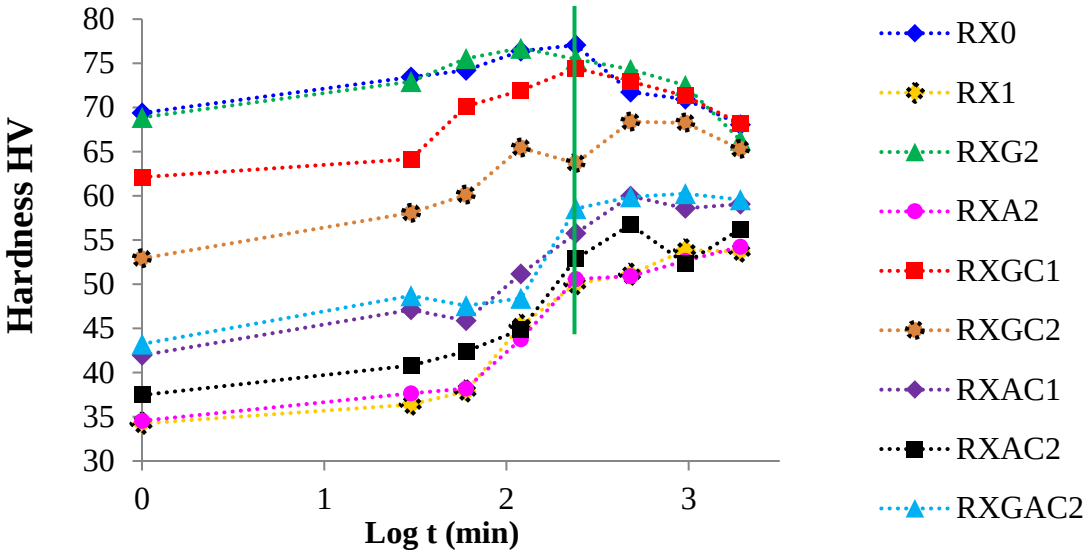

Fig. 2 Hardness (HV) as a function of time for the nine alloys, during an artificial ageing (AA) at 195 °C (see Fig. 1). The lean reference, RX1, exhibits the lowest HV while the denser reference, RX0, has the highest HV values together with RXG2. The green vertical line indicates the conditions investigated by TEM, corresponding to 4 hours of AA.

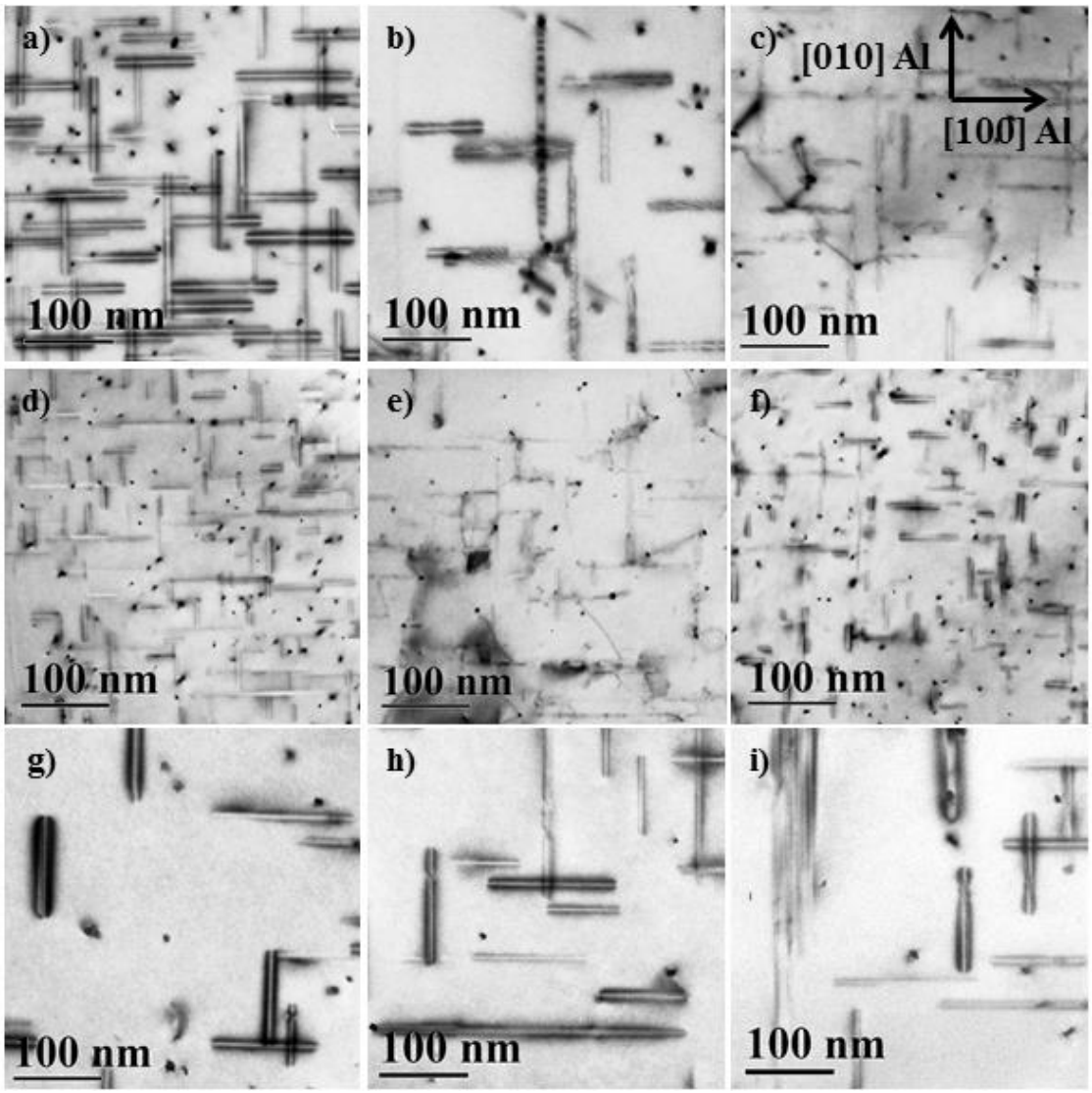

Fig. 3 TEM bright field images from representative areas in the alloys after 4 hours of AA at 195 °C. The respective images are from a) RX0, b) RX1, c) RXGAC2, d) RXG2, e) RXGC1, f) RXGC2, g) RXAC1, h) RXAC2 and i) RXA2. a) – c) and g) – i) have thicknesses of approximately 150 nm and are therefore directly comparable. d) – f) have thicknesses of about 70 nm.

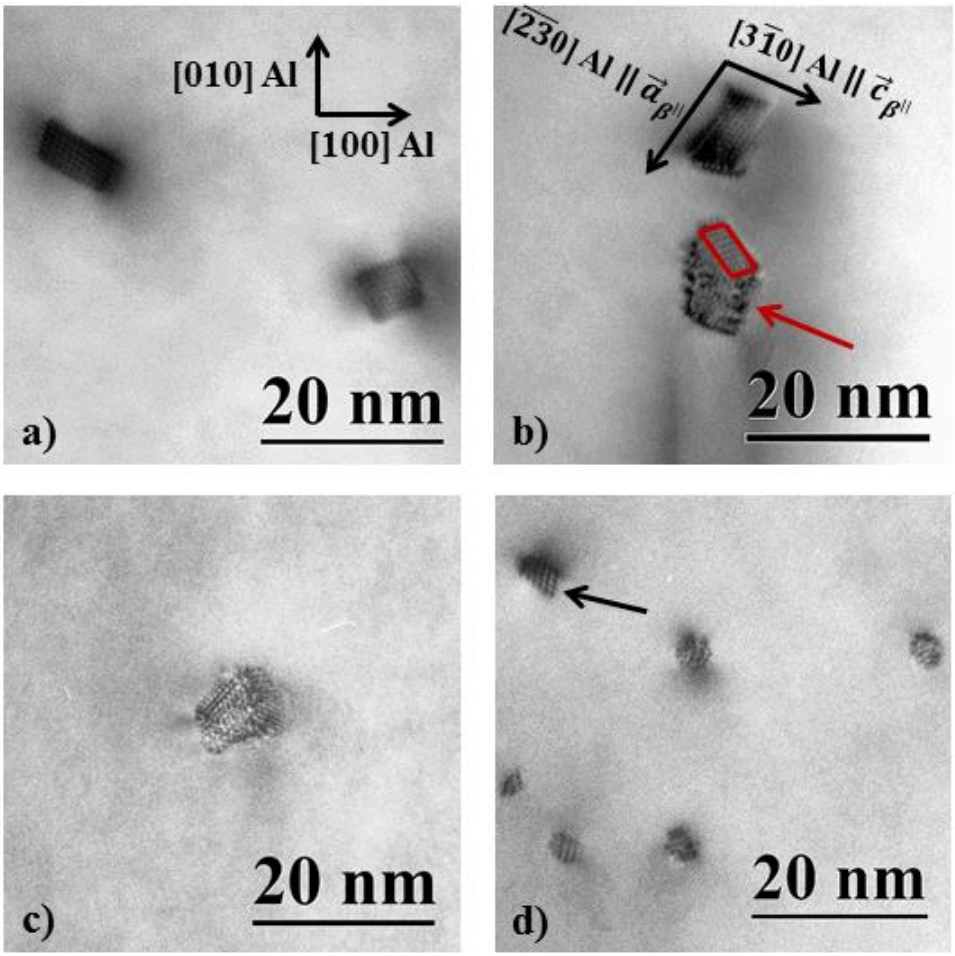

Fig. 4 TEM bright field images of precipitate cross sections from four selected alloys: a) RX0, b) RX1, c) RXA2 and d) RXG2. All images are taken along the same zone axis, as shown in a). Both precipitates in a) have *β''* periodicities. The black arrows in b) indicate the crystallographic orientation of the respective *β''* with the Al matrix. The area outlined in red in b) marks the *β''* part of a precipitate which also contains a disordered part shown by the red arrow. The precipitate in c) is composed of parts with different structures in the same needle. Most precipitates in d) are disordered, except the one indicated by the black arrow, which has *β''* periodicity.

Table 2 Calculated average precipitate cross sections (CS), needle lengths, number densities and volume fractions with corresponding errors. The Vickers Hardness (HV) for each condition is also given in the rightmost column. The volume fraction of precipitates has a 95 % probability of being within the intervals shown.

Alloy	CS [nm^2]	Needle length [nm]	Number Density [$\#/\mu m^{-3}$]	Volume Fraction [%]	HV
RX0	24 ± 2	95 ± 5	3 200 ± 400	{0.64, 0.80}	77.0
RX1	42 ± 4	243 ± 73	170 ± 50	{0.12, 0.19}	50.0
RXGC1	12 ± 1	57 ± 8	8 300 ± 1 300	{0.48, 0.62}	74.5
RXAC1	30 ± 3	118 ± 16	1 900 ± 300	{0.55, 0.75}	55.8
RXG2	7 ± 1	37 ± 1	13 200 ± 1 400	{0.25, 0,41}	75.5
RXGC2	9 ± 2	39 ± 5	11 200 ± 1 400	{0.33, 0.42}	63.7
RXA2	63 ± 8	211 ± 44	400 ± 90	{0.41, 0.63}	50.6
RXAC2	47 ± 5	170 ± 19	370 ± 50	{0.25, 0.33}	52.9
RXGAC2	30 ± 2	124 ± 25	1 700 ± 360	{0.46, 0.67}	58.5

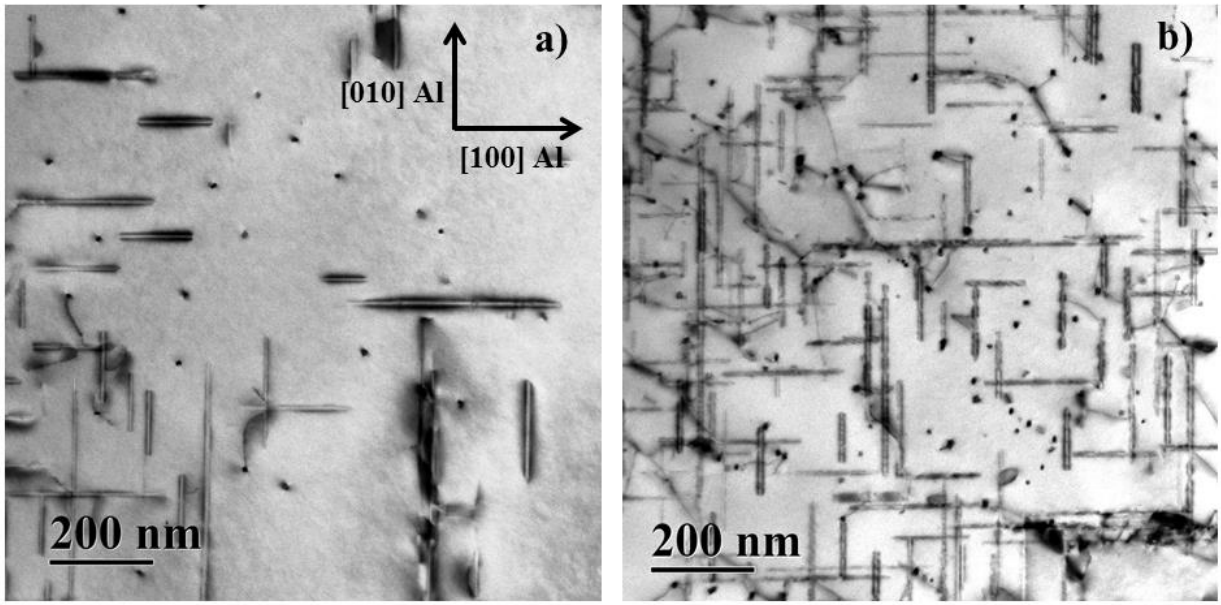

Fig. 5 TEM bright field images from two different areas in the lean reference alloy RX1. The images are examples of areas with predominately large needles (a) and of areas with a finer distribution of smaller needles (b).

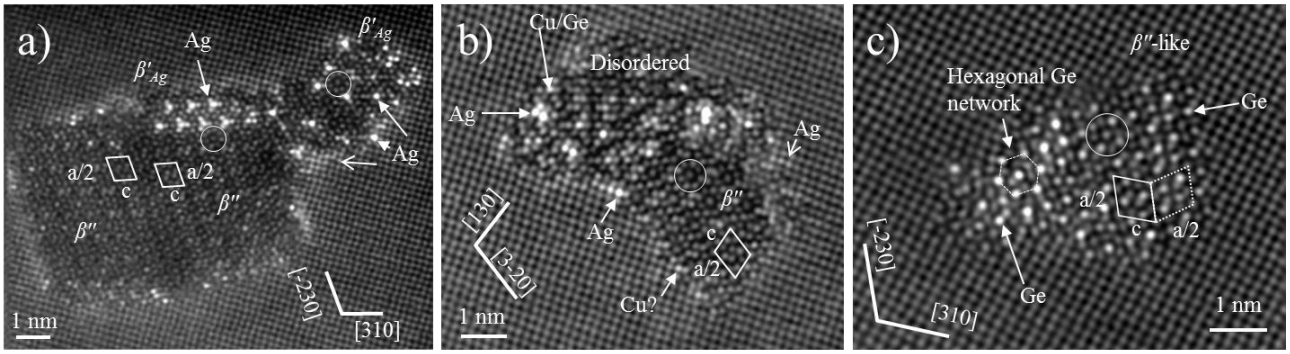

Fig. 6 HAADF images of typical precipitates in three of the investigated alloys, showing that formation of *β''* phase is strongly affected by the additions of Ge, Ag, and Cu. Circles indicate basic units of *β''*. Open/filled arrows point to single columns/areas. Half unit-cells of *β''* are indicated: (a) Silver-containing alloy RXA2 with large Ag-free *β''* particle with a central stacking fault along the *a*-axis. Ag is found at the interface as single columns, ordered in a β'_{Ag} phase, or in a low concentration in Al just outside the particle, (b) Mixed *β''*/disordered particle in alloy RXGAC2 with additions of Ge, Ag and Cu. The added elements observed in the disordered part, cannot be distinguished by the Z-contrast alone. (c) Alloy RXG2 with Ge addition. Ge integrates in the *β''* structure, substituting in some of the Si-positions in the *β''* phase unit, leading to disorder / restacking of the units (dotted rhomb). The left part shows a region where Ge arranges hexagonally.

4 Conclusions

Improving extrusion speed in 6000 Al alloys while maintaining initial strength has been the objective of this work. In order to do this, the total amount of solute in the alloys was reduced. The (Mg + Si) amount was lowered and combinations of Ag, Ge and Cu were back-added in smaller quantities. In total, nine alloys were investigated. One alloy was kept as a "dense reference". A lean reference had 16.7 % of the solute atoms removed as compared to the dense reference. The remaining seven alloys had low additions of one or more element of Ge, Ag and Cu, in total less than 0.05 at % added amount.

The microstructure evolution of the nine alloys was investigated by hardness measurements, transmission electron microscopy (TEM) and high angle annular dark field scanning TEM (HAADF STEM). The precipitate microstructures were quantified by TEM after identical heat-treatments (4 hours of artificial aging at 195 °C), which corresponded to peak hardness for the three strongest alloys.

The microstructure of the leanest reference was inhomogeneous, with grains consisting of regions with homogeneously distributed precipitates together with regions with coarse precipitates mainly found on dislocations. All the other alloys had microstructures dominated by a more homogeneous nucleation of hardening precipitates.

Alloys containing Ge, but no Ag, were found to have high hardness. The alloy containing only Ge and no Ag or Cu was the only alloy competing with the dense reference alloy in hardness. The high hardness corresponds well with the microstructure consisting of a fine dispersion of small and short needles. Most precipitates found in the Ge-containing alloys were disordered, partly consisting of a hexagonal ordering of Ge columns. Ge was found to integrate in the structure of β'', substitute Si positions and cause regions with disorder in the stacking of the β'' unit. It is proposed in this work that since Ge chemically resembles Si, it too causes the hexagonal Si/Ge network to form. In addition, Ge is believed to have a higher vacancy binding energy than the other elements discussed. All over, the β'' phase is strongly affected by the additions of Ge, Ag and Cu.

The Ag-added alloy had the least total solute, hence, when comparing solute amounts to precipitate statistics and hardness, silver shows some benefit to precipitation and strengthening of the material. Large Ag-free β'' particles were found in this alloy, together with particles containing Ag at the interfaces as single columns. The β'_{Ag} phase was also frequently observed.

Replacing Ag with some Cu in the Ag-containing alloys resulted in a significant refinement of precipitates. Cross sections were reduced in size and the number density increased by at least a factor of 5. The additions seem to relate well with the idea of stronger solute- vacancy bonding and correlate with finer and more precipitates. When replacing some Ge with Cu in the Ge-added alloys a drop in hardness was observed. The decrease in hardness is seen as a direct consequence of the reduction of Ge. In these alloys Cu does not refine cross sections much.

It is proposed that the elements' ability to bind vacancies is significant for the nucleation process of precipitates. As Ge binds vacancies more than Si and all the other alloying elements in these alloys, Ge will produce more favorable nucleation sites for precipitates, leading to an increased precipitate number density after heat treatment. Mg has the lowest ability to bind vacancies of the elements discussed. It is suggested that Mg has a stronger adherence to Ge-containing clusters than to those only containing Si. Consequently, the Ge-added alloy solves the initial problem of lowering solute additions while maintaining strength.

Acknowledgements

This work has been supported through the BIA RolEx project, no. 219371 by Hydro Aluminium and the Research Council of Norway. The contributors are greatly acknowledged for their support. The authors would also like to thank Birgitte Karlsen, SINTEF Materials and Chemistry for performing heat treatments and hardness measurements of the alloys.

References

[1] D. McLeod: *Mechanical Properties of Metals*, p.162, John Wiley & sons Inc, New York, 1962.

[2] C.D. Marioara, H. Nordmark, S.J. Andersen, R. Holmestad: *J. Mater. Sci.*, 2006, vol. 41, pp. 471 – 478.

[3] G. A. Edwards, K. Stiller, G. L. Dunlop, M. J. Couper: *Acta Mater.* , 1998, vol. 46, pp. 3893 – 3904.

[4] C. D. Marioara, S. J. Andersen, J. Jansen, H. W. Zandbergen: *Acta Mater.*, 2001, vol. 49, pp. 321 – 328.

[5] S. J. Andersen, H. W. Zandbergen, J. Jansen, C. Træholt, U. Tundal, O. Reiso: *Acta Mater.*, 1998, vol. 46, pp. 3283 – 3298.

[6] H. S. Hasting, A. G. Frøseth, S. J. Andersen, R. Vissers, J. C. Walmsley, C. D. Marioara, F. Danoix, W. Lefebvre, R. Holmestad: *J. Appl. Phys.*, 2009, vol. 106, nbr. 123527.

[7] R. Vissers, M. A. van Huis, J. Jansen, H. W. Zandbergen, C. D. Marioara, S. J. Andersen: *Acta Mater.*, 2007, vol. 55, pp. 3815 – 3823.

[8] S. J. Andersen, C. D. Marioara, R. Vissers, A. Frøseth, H. W. Zandbergen: *Mater. Sci. Eng. A*, 2007, vol. 444, pp. 157 – 169.

[9] S. J. Andersen, C. D. Marioara, A. Frøseth, R. Vissers, H. W. Zandbergen: *Mater. Sci. Eng. A*, 2005, vol. 390, pp. 127 – 138.

[10] R. Vissers, C. D. Marioara, S. J. Andersen, R. Holmestad: *Aluminium Alloys*, vol. 2, 2008, pp. 1263 – 1269.

[11] K. Teichmann, C. D. Marioara, S. J. Andersen, K. Marthinsen: *Met. Mater. Trans. A*, 2012, vol. 43, pp. 4006-4014.

[12] T. Saito, S. Muraishi, C. D. Marioara, S. J. Andersen, J. Røyset, R. Holmestad: *Met. Mater. Trans. A*, 2013, vol. 44, pp. 4124 – 4135.

[13] C. D. Marioara, S. J. Andersen, T. N. Stene, H. Hasting, J. C. Walmsley, A. T. J. van Helvoort, R. Holmestad: *Philos. Mag.*, 2007, vol. 87, p. 3385.

[14] D. J. Chakrabarti and D. E. Laughlin: *Prog. Mater. Sci.*, 2004, vol. 49, p. 389.

[15] C. Cayron, L. Sagalowicz, O. Beffort, P. A. Buffat: *Philos. Mag. A*, 1999, vol. 79, p. 2833.

[16] K. Matsuda, Y. Uetani, T. Sato, S. Ikeno (2001): *Metall. Mater. Trans. A*, 2001, vol. 32, p. 1293.

[17] H. Zhan, J. M. C. Mol, F. Hannour, L. Zhuang, H. Terryn, J. H. W. de Wit: *Materials and Corrosion*, 2008, vol. 59, pp. 670 – 675.

[18] G. Svenningsen, J. Lein, A. Bjørgum, J. H. Nordlien, Y. Yu, K. Nisancioglu: *Corros. Sci.*, 2006, vol. 48, pp. 226 – 242.

[19] G. Svenningsen, M. H. Larsen, J. C. Walmsley, J. H. Nordlien, K. Nisancioglu: *Corros. Sci.*, 2006, vol. 48, pp. 1528 – 1543.

[20] J. Kim, C. D. Marioara, R. Holmestad, E. Kobayashi, T. Sato: *Mater. Sci. Eng. A*, 2013, vol. 560, pp. 154 – 162.

[21] C. D. Marioara, S. J. Andersen, J. Røyset, O. Reiso, S. Gulbrandsen-Dahl, T. E. Nicolaisen, I. E. Opheim, J. F. Helgaker, R. Holmestad: *Metall. Mater. Trans A*, 2014, vol. 45, pp. 2938 – 2949.

[22] J.-H. Kim, E. Kobayashi, T. Sato: *Mater. Trans.*, 2011, vol. 52, pp. 906 – 913.

[23] J.-H. Kim, H. Tezuka, E. Kobayashi, T. Sato: *Kor. J. Mater. Res.*, 2012, vol. 22, pp. 329 – 334.

[24] M. Mihara, E. Kobayashi, T. Sato: *Mater. Sci. For.*, 2014, vol. 794-796, pp. 996 – 1001.

[25] L. Arnberg, B. Aurivillius: *Acta Chem. Scand.A*, 1980, vol. 34, p. 1.

[26] T. Saito, C. D. Marioara, S. J. Andersen, W. Lefebvre, R. Holmestad: *J. Phys*., 2014, Conf. Ser. 522 012030.

[27] F. J. H. Ehlers, S. Wenner, S. J. Andersen, C. D. Marioara, W. Lefebvre, C. B. Boothroyd, R. Holmestad: *J. Mater. Sci.*, 2014, vol. 49, pp. 6413-6426.

[28] J. M. Silcock, T. J. Heal: *Acta Cryst*., 1956, vol. 9, p. 680.

[29] I. J. Polmear: *Light Alloys "From Traditional Alloys to Nanocrystals"*, second edition, pp. 43-51, Butterworth-Heinemann publications, UK, 2006.

[30] I. J. Polmear: *Nature*, 1960, vol. 186, p. 303.

[31] M. Kubota, J. F. Nie, B. C. Muddle: *Mater. Trans.*, 2012, vol. 45, pp. 3256 – 3263.

[32] L. Bourgeois, C. Dwyer, M. Weyland, J.-F. Nie, B. C. Muddle: *Acta Mater.*, 2011, vol. 59, pp. 7043 – 7050.

[33] J. M. Rosalie, C. Dwyer, L. Bourgeois: *Acta Mater.*, 2014, vol. 69, pp. 224 – 235.

[34] C. D. Marioara, J. Nakamura, K. Matsuda, S. J. Andersen, R. Holmestad, T. Sato, T. Kawabata, S. Ikeno: *Phil. Mag.*, 2012, vol. 92, pp. 1149 – 1158.

[35] J. M. Rosalie, L. Bourgeois, B. C. Muddle: *Phil. Mag.*, 2009, vol. 89, pp. 2195 – 2211.

[36] K. Matsuda, J. Nakamura, T. Kawabata, S. Ikeno, T. Sato, C. D. Marioara, S. J. Andersen, R. Holmestad: *Mater. Sci. Forum*, 2012, vol. 706-709, pp. 357 – 360.

[37] K. Matsuda, S. Ikeno, T. Munekata: *Mater. Sci. Forum.*, 2006, vol. 519 – 521, p. 221.

[38] R. Bjørge, C. D. Marioara, S. J. Andersen, R. Holmestad: *Metall. Mater. Trans. A*, 2010, vol. 41, pp. 1907 – 1916.

[39] R. Bjørge, S. J. Andersen, C. D. Marioara, J. Etheridge, R. Holmestad: *Phil. Mag.*, 2012, vol. 92, pp. 3983 – 3993.

[40] P. B. Hirsch, J. Silcox, R. E. Smallman, K. H. Westmacott: *Phil. Mag.*, 1958, vol. 3, pp. 897 – 908.

[41] S. Yoshida, Y. Shimomura, M. Kiritani: *Journal of the Physical Society of Japan*, 1962, vol. 17, pp. 1196 – .

[42] V. Gavini, K. Bhattacharya, M. Ortiz: *Phys. Rev. B*, 2007, vol. 76, 180101.

[43] L. A. Westfall: *An investigation of nano-voids in quenched aluminum by small-angle x-ray scattering*, 2008, MSci thesis, Queen's University, Kingston, Ontario, Canada.

[44] C. Wolverton: *Acta Mater.*, 2007, vol. 55 (2007), pp. 5867 – 5872.

[45] L. Reich, M. Murayama, K. Hono: *Acta Mater.*, 1998, vol. 46, pp. 6053 – 6062.

[46] U. Tundal, O. Reiso, E. Hoff, R. Dickson, C. Devadas: *Proc. 10th International Aluminum Extrusion Technology Seminar*, May 15-18, 2012, Miami, FL, USA, vol. II, pp. 21 – 33.

[47] C. D. Marioara, S. J. Andersen, H. W. Zandbergen, R. Holmestad: *Metall. Mat. Trans. A*, 2005, vol. 36, pp. 691 – 702.

[48] K. Teichmann, C. D. Marioara, S. J. Andersen, K. Marthinsen: *Mater. Charact.*, 2013, vol. 75, pp. 1 – 7.

[49] G. P. M. Leyson, L. G. Hector Jr., W. A. Curtin, *Acta Mater.*, 2012, vol. 60, pp. 3873 – 3884.

[50] T. Saito, C. D. Marioara, J. Røyset, K. Marthinsen, R. Holmestad: *Mater. Sci. Eng. A*, 2014, vol. 609, pp. 72 – 79.